A Physically-Based Night Sky Model

Henrik Wann Jensen[1] Frédo Durand[2] Michael M. Stark[3] Simon Premože[3]
Julie Dorsey[2] Peter Shirley[3]

[1]Stanford University [2]Massachusetts Institute of Technology [3]University of Utah

Abstract

This paper presents a physically-based model of the night sky for realistic image synthesis. We model both the direct appearance of the night sky and the illumination coming from the Moon, the stars, the zodiacal light, and the atmosphere. To accurately predict the appearance of night scenes we use physically-based astronomical data, both for position and radiometry. The Moon is simulated as a geometric model illuminated by the Sun, using recently measured elevation and albedo maps, as well as a specialized BRDF. For visible stars, we include the position, magnitude, and temperature of the star, while for the Milky Way and other nebulae we use a processed photograph. Zodiacal light due to scattering in the dust covering the solar system, galactic light, and airglow due to light emission of the atmosphere are simulated from measured data. We couple these components with an accurate simulation of the atmosphere. To demonstrate our model, we show a variety of night scenes rendered with a Monte Carlo ray tracer.

Keywords: Natural Phenomena, Atmospheric Effects, Illumination, Rendering, Ray Tracing

ACM SIGGRAPH 2001, 12-17 August 2001, Los Angeles, CA, USA

1 Introduction

In this paper, we present a physically-based model of the night sky for image synthesis, and demonstrate it in the context of a Monte Carlo ray tracer. Our model includes the appearance and illumination of all significant sources of natural light in the night sky, except for rare or unpredictable phenomena such as aurora, comets, and novas.

The ability to render accurately the appearance of and illumination from the night sky has a wide range of existing and potential applications, including film, planetarium shows, drive and flight simulators, and games. In addition, the night sky as a natural phenomenon of substantial visual interest is worthy of study simply for its intrinsic beauty.

While the rendering of scenes illuminated by daylight has been an active area of research in computer graphics for many years, the simulation of scenes illuminated by nightlight has received relatively little attention. Given the remarkable character and ambiance of naturally illuminated night scenes and their prominent role in the history of image making — including painting, photography, and cinematography — this represents a significant gap in the area of realistic rendering.

1.1 Related Work

Several researchers have examined similar issues of appearance and illumination for the daylight sky [6, 19, 30, 31, 34, 42]. To our knowledge, this is the first computer graphics paper that describes a general simulation of the nighttime sky. Although daytime and nighttime simulations share many common features, particularly

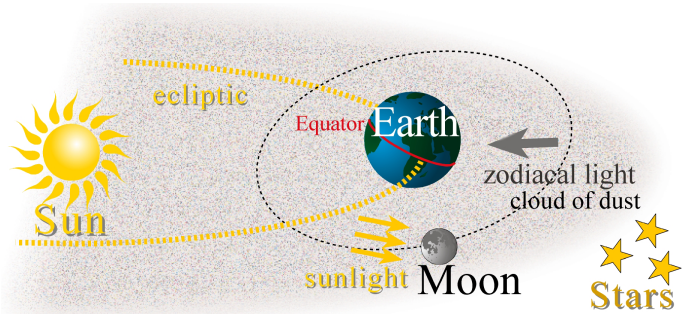

Figure 1: Elements of the night sky. Not to scale.

the scattering of light from the Sun and Moon, the dimmer nighttime sky reveals many astronomical features that are invisible in daytime and thus ignored in previous work. Another issue unique to nighttime is that the main source of illumination, the Moon, has its own complex appearance and thus raises issues the Sun does not. Accurately computing absolute radiances is even more important for night scenes than day scenes. If all intensities in a day scene are doubled, a tone-mapped image will change little because contrasts do not change. In a night scene, however, many image features may be near the human visibility threshold, and doubling them would move them from invisible to visible.

Some aspects of the night sky have been examined in isolation. In a recent paper, Oberschelp and Hornug provided diagrammatic visualizations of eclipses and planetary conjunction events [32]. Their focus is the illustration of these events, not their realistic rendering. Researchers have created detailed models of the appearance of Saturn [3, 4] and Jupiter [47]. These models were intended for simulation of space scenes and would be overkill for renderings of Earth scenes. Baranoski et al. did a careful simulation of the aurora borealis [1]. Although we do not simulate aurora phenomena in our model, the techniques of Baranoski et al. could be added seamlessly to our simulations because aurora are an emission phenomenon with little correlation to the Earth's position relative to the Sun, and thus can be added independently to other nighttime effects.

1.2 Overview

The next section introduces the components of our model. Section 3 describes astronomical models to compute the accurate positions of the elements of the night sky in a framework appropriate for use in computer graphics. Sections 4–6 introduce our approach for modeling and rendering the key sources of illumination in the night sky. We discuss our implementation and results in Section 7. Finally we conclude in Section 8 with some discussion and directions for future work.

2 Sources of Night Illumination

To create realistic images of night scenes, we must model the characteristics of nighttime illumination sources, both in terms of their contribution to the scene, and their direct appearance in the sky. These sources are illustrated in Figures 1 and 2 and summarized below.

- **The Moon.** Most of the visible moonlight is actually sunlight, incident on the Moon and scattered from its surface in all directions. Light received directly from the Moon and moonlight scattered by the atmosphere account for most of the available light at night. The appearance of the Moon itself is important in the night sky due to its proximity to and visibility from the Earth.

Component	Irradiance $[W/m^2]$
Sunlight	$1.3 \cdot 10^{3}$
Full Moon	$2.1 \cdot 10^{-3}$
Bright planets	$2.0 \cdot 10^{-6}$
Zodiacal light	$1.2 \cdot 10^{-7}$
Integrated starlight	$3.0 \cdot 10^{-8}$
Airglow	$5.1 \cdot 10^{-8}$
Diffuse galactic light	$9.1 \cdot 10^{-9}$
Cosmic light	$9.1 \cdot 10^{-10}$

Figure 2: Typical values for sources of natural illumination at night.

- **The Sun.** The sunlight scattered around the edge of the Earth makes a visible contribution at night. During "astronomical twilight" the sky is still noticeably bright. This is especially important at latitudes greater than 48° N or S, where astronomical twilight lasts all night in midsummer.

- **The planets and stars.** Although the light received from the stars is important as an illumination source only on moonless nights, the appearance of stars in the sky is crucial for night scenes. The illumination and appearance of the other planets are comparable to that of bright stars.

- **Zodiacal light.** The solar system contains dust particles that scatter sunlight toward the Earth. This light changes the appearance and the illumination of the night sky.

- **Airglow.** The atmosphere has an intrinsic emission of visible light due to photochemical luminescence from atoms and molecules in the ionosphere. This accounts for one sixth of the light in the moonless night sky.

- **Diffuse galactic and cosmic light.** Light from galaxies other than the Milky Way.

The atmosphere also plays an important role in the appearance of the night sky. It scatters and absorbs light and is responsible for a significant amount of indirect illumination.

In general, the above sources cannot be observed simultaneously in the night sky. In particular, the dimmest phenomena can only be seen on moonless nights. In fact, the various components of night light are only indirectly related to one another; hence, we treat them separately in our model.

2.1 Model Overview

The main components of our model are illustrated Figure 3 and outlined below. Subsequent sections will discuss each of these components in greater detail.

Our general approach is to model the direct appearance of the celestial elements and the illumination they produce differently, as the latter requires less accuracy and a simpler model is easier to integrate and introduces less variance. We demonstrate our model in a spectral rendering context; however the data can be converted to the CIE XYZV color space (including a scotopic component V for rod vision).

- **Astronomical positions.** We summarize classical astronomical models and provide a simplified framework to compute accurate positions of the Sun, Moon, and stars.

- **Moon.** The Moon is simulated as explicit geometry illuminated by two directional light sources, the Sun and the Earth. We include a model based on elevation and albedo data of the surface of the Moon, and on a specialized BRDF description. A simpler model is presented for the illumination from the Moon.

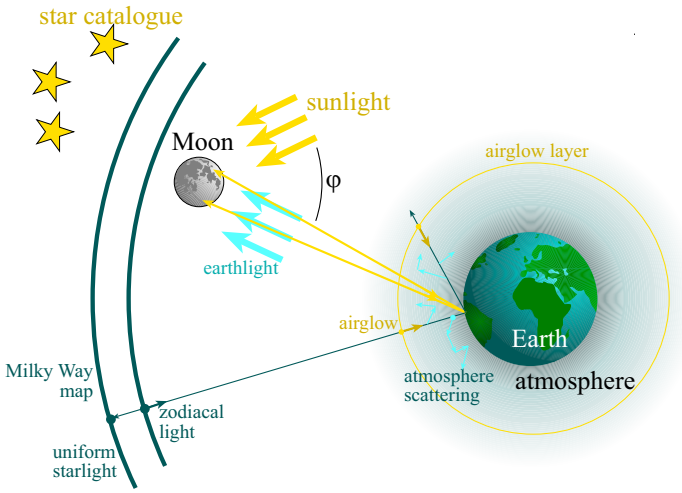

Figure 3: Components of the night sky model.

- **Stars.** The appearance of the brightest stars is simulated using data that takes into account their individual position, magnitude and temperature. Planets are displayed similarly, albeit by first computing their positions. Star clouds — elements that are too dim to observe as individual stars but collectively produce visible light — including the Milky Way, are simulated using a high resolution photograph of the night sky processed to remove the bright stars. Illumination from stars is treated differently, using a simple constant model.

- **Other astronomical elements.** Zodiacal light, atmospheric airglow, diffuse galactic light, and cosmic lights are simulated using measured data.

- **Atmospheric scattering.** We simulate multiple scattering in the atmosphere due to both molecules and aerosols.

3 Astronomical Positions

We introduce classical astronomical formulas to compute the position of various celestial elements. For this, we need to review astronomical coordinate systems. This section makes simplifications to make this material more accessible. For a more detailed description, we refer the reader to classic textbooks [7, 10, 23, 24] or to the year's *Astronomical Almanac* [44].

All of the formulas in the Appendix have been adapted from high accuracy astronomical formulas [23]. They have been simplified to facilitate subsequent implementation, as computer graphics applications usually do not require the same accuracy as astronomical applications. We have also made conversions to units that are more familiar to the computer graphics community. Our implementation usually uses higher precision formulas, but the error introduced by the simplifications is lower than 8 minutes of arc over five centuries.

3.1 Coordinate Systems

The basic idea of positional astronomy is to project everything onto *celestial spheres*. Celestial coordinates are then spherical coordinates analogous to the terrestrial coordinates of longitude and latitude. We will use three coordinate systems (Figure 4) — two centered on the Earth (equatorial and ecliptic) and one centered on the observer (horizon). Conversion formulas are given in the Appendix.

The final coordinate system is the local spherical frame of the observer (horizon system). The vertical axis is the local zenith, the

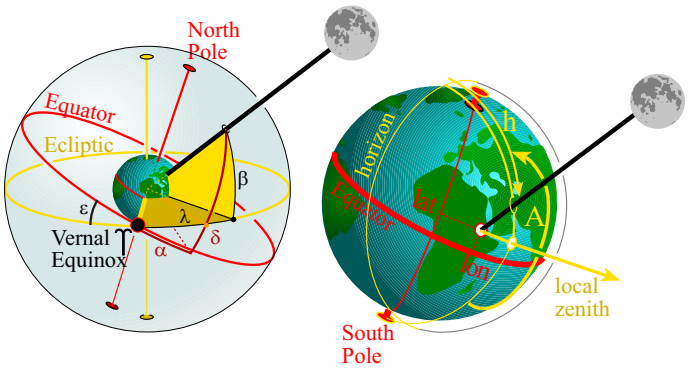

Figure 4: Coordinate systems. Left: equatorial (α, δ) and ecliptic (λ, β). Right: Local coordinates (A, h) for an observer at longitude lon and latitude lat.

latitude is the altitude angle h above the horizon, and the longitude, or azimuth A, is measured eastward from the south direction (Figure 4).

The two other systems are centered on the Earth but do not depend on its rotation. They differ by their vertical axis, either the North pole (and thus the axis of rotation of the Earth) for the equatorial system, or the normal to the ecliptic, the plane of the orbit of the Earth about the Sun, for the ecliptic system (Figures 1 and 4).

The Earth's rotational axis remains roughly parallel as the Earth orbits around the Sun (the angle between the ecliptic and the Equator is about $23.44°$). This means that the relationship between the angles of the two systems does not vary. In both cases, the reference for the longitude is the Vernal Equinox, denoted ♈, which corresponds to the intersection of the great circles of the Equator and the ecliptic (Figure 4).

However, the direction of the axis of the Earth is not quite constant. Long-term variations known as *precession* and short-term oscillations known as *nutations* have to be included for high accuracy, as described in the Appendix.

3.2 Position of the Sun

The positions of the Sun and Moon are computed in ecliptic coordinates (λ, β) and must be converted using the formulas in Appendix. We give a brief overview of the calculations involved. Formulas exhibit a mean value with corrective trigonometric terms (similar to Fourier series).

The ecliptic latitude of the Sun should by definition be $\beta_{\mathrm{Sun}} = 0$. However, small corrective terms may be added for very high precision, but we omit them since they are below $10''$.

3.3 The Moon

The formula for the Moon is much more involved because of the perturbations caused by the Sun. It thus requires many corrective terms. An error of $1°$ in the Moon position corresponds to as much as 2 diameters. We also need to compute the distance d_{Moon}, which is on average 384 000 km. The orbital plane of the Moon is inclined by about $5°$ with respect to the ecliptic. This is why solar and lunar eclipses do not occur for each revolution and are therefore rare.

The Moon orbits around the Earth with the same rotational speed as it rotates about itself. This is why we always see nearly the same side. However, the orbit of the Moon is not a perfect circle but an ellipse (eccentricity about 1/18), and its axis of revolution is slightly tilted with respect to the plane of its orbit (Figure 5). For this reason, about 59% of the lunar surface can be seen from the Earth. These apparent oscillations are called *librations* and are

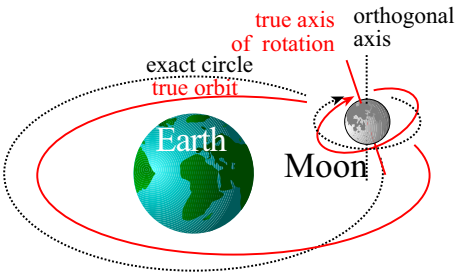

Figure 5: (a) Librations of the Moon are due to the eccentricity of its orbit and to the tilt of its axis of rotation. (b) Angle for the BRDF of the Moon.

included in our model as a result of our direct modeling approach. (See the Appendix for formulas.)

3.4 Position of Stars

For the stars, we used the Yale Bright Star Catalog [14]. It contains about 9000 stars, including the roughly 6000 visible to the naked eye. The stellar positions are given in equatorial coordinates. The catalogue contains the position for 2000 A.D. and the *proper motion* of stars, caused by their rectilinear motion through space. The position of a star for a given date is then computed using a linear approximation, usually in rectangular coordinates (the apparent motion can be neglected if the date is less than 5 centuries from 2000 A.D.). The positions of the planets are computed using formulas similar to those used for the Moon and the Sun [23].

4 Moonlight

The large-scale topography of the Moon is visible from the Earth's surface, so we render its direct appearance using a geometric model containing elevation and albedo illuminated by two directional light sources, the Earth and the Sun.

4.1 Modeling the Moon

To model the Moon accurately, we use the positions computed in the previous section and measured data of the lunar topography and albedo [27]. The Moon is considered a poor reflector: on average only 7.2% of the light is reflected [20]. The albedo is used to modulate a BRDF model, which we present in the next section. The elevation is measured with a precision of a quarter of a degree in longitude and latitude (1440×720), and the albedo map has size 800×400.

The Moon is illuminated by the Sun, which can be treated as a directional light source. We use the positions of the Moon and Sun to determine the direction of illumination. The Sun is modeled as a black body at temperature $5900K$ (see Appendix for conversion), and power $1905 \frac{W}{m^2}$. The Sun appears about 1.44 times brighter from the Moon than from the surface of the Earth because of the absence of atmosphere. We do not include the Earth as an occluder, which means we cannot simulate lunar eclipses. This could easily be done by modeling the Sun as a spherical light source to simulate penumbra.

The faint light visible on the dark side of the Moon when it is a thin crescent is known as *earthshine*. Earthshine depends strongly on the phase of the Earth. When the Earth is full (at new Moon), it casts the greatest amount of light on the Moon, and the earthshine is relatively bright and easily observed by the naked eye. We model earthshine explicitly by including the Earth as a second light source for the Moon surface.

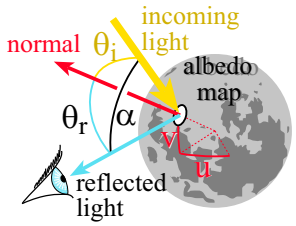

Figure 6: Angle for the BRDF of the Moon.

Accuracy is not crucial for earthshine except for the new Moon, so we simply use the percentage of lit Earth visible from the Moon and multiply it by the intensity of the full earthshine, which is $0.19 \frac{W}{m^2}$. Given the Earth phase, that is, the angle $\pi - \varphi$ between the Moon and the Sun as seen from the Earth (the opposite of the Moon phase φ), we obtain [46]:

$$E_{em} = 0.19{*}0.5 \left[1 - \sin(\frac{\pi - \varphi}{2}) \tan(\frac{\pi - \varphi}{2}) \ln(\cot(\frac{\pi - \varphi}{4}))\right] \quad (1)$$

4.2 BRDF of the Moon

The Moon has a low albedo and a reddish color, and it exhibits backscattering reflection (it is much brighter at full Moon) [11]. Furthermore, the apparent disc of the full Moon has a remarkable photometric property: its average brightness at the center is the same as at the edge [11]. The Moon is therefore said to exhibit no *limb darkening*. This can be explained by the pulverized nature of its surface. We use the complete Hapke-Lommel-Seeliger model of the reflectance function of the Moon, which provides a good approximation to the real appearance and a good fit to measured data [12]. The BRDF f consists of a retrodirective function B and a scattering function S. As the BRDF of the Moon is rather uniform, but the albedo is variable, we model them independently. We multiply the BRDF by the albedo and by the spectrum of the Moon.

The geometry for the BRDF is summarized in Figure 6. φ is the lunar phase angle (angle Sun-Earth as seen from the Moon, or equivalently for our purpose, the angle between incident and reflected light). θ_r is the angle between the reflected light and the surface normal; θ_i is the angle between the incident light and the surface normal.

Note that to compute the contribution of the earthshine, the Sun has to be replaced by the Earth using Equation 1 for the intensity. φ is then null by definition.

The BRDF, f, of the Moon can be computed with:

$$f(\theta_i, \theta_r, \varphi) = \frac{2}{3\pi} B(\varphi, g) S(\varphi) \frac{1}{1 + \cos\theta_r / \cos\theta_i}. \quad (2)$$

The retrodirective function $B(\varphi, g)$ is given by

$$B(\varphi, g) = \begin{cases} 2 - \frac{\tan\varphi}{2g} \left(1 - e^{-g/\tan\varphi}\right) \left(3 - e^{-g/\tan\varphi}\right), & \varphi < \pi/2 \\ 1, & \varphi \geq \pi/2, \end{cases} \quad (3)$$

where g is a surface density parameter which determines the sharpness of the peak at the full Moon. We use $g = 0.6$, although values between 0.4 (for rays) and 0.8 (for craters) could be used.

The scattering law S for individual objects is given by [12]:

$$S(\varphi) = \frac{\sin|\varphi| + (\pi - |\varphi|)\cos|\varphi|}{\pi} + t\left(1 - \frac{1}{2}\cos|\varphi|\right)^2, \quad (4)$$

where t introduces a small amount of forward scattering that arises from large particles that cause diffraction [37]. $t = 0.1$ is a good fit to Rougier's measurements [16] of the light from the Moon.

The spectrum of the Moon is distinctly redder than the Sun's spectrum. Indeed, the lunar surface consists of a layer of a porous pulverized material composed of particles larger than the wavelengths of visible light. As a consequence and in accordance with the Mie theory [45], the albedo is approximately twice as large for red (longer wavelengths) light than for blue (shorter wavelengths) light. In practice, we use a spectral reference that is a normalized linear ramp (from 70% at 340nm to 135% at 740nm). In addition, light scattered from the lunar surface is polarized, but we do not include polarization in our model. Figure 7 demonstrates our Moon model for various conditions.

4.3 Illumination from the Moon

For illumination coming from the Moon, it is sufficient to use a simple directional model since the Moon is very distant. This moreover introduces less variance in the illumination integration.

Using the Lommel-Seeliger law [46], the irradiance E_m from the Moon at phase angle φ and a distance d can be expressed as:

$$E_m(\varphi, d) = \frac{2\ C\ r_m^2}{3\ d^2} \left\{ E_{em} + E_{sm} \left(1 - \sin\tfrac{\varphi}{2} \tan\tfrac{\varphi}{2} \log\left(\cot\tfrac{\varphi}{4}\right)\right)\right\}, \tag{5}$$

where r_m is the radius of the Moon, E_{sm} is the irradiance from the Sun at the surface of the Moon, and E_{em} is the earthshine contribution as computed from Equation 1. Recall that the phase angle of the Moon with respect to earthshine is always null. The normalizing constant C is the average albedo of the Moon ($C = 0.072$).

5 Starlight

Stars are important visual features in the sky. We use actual star positions (as described in Section 3.4), and brightnesses and colors from the same star catalogue [14]. In this section, we describe how stars are included in our model, present the calculation of their brightness and chromaticity, and finally, discuss the illumination coming from stars.

5.1 Rendering Stars

Stars are very small, and it is therefore not practical to use explicit ray tracing to render them as rays would easily miss them. Instead, we use an image-based approach in which a separate star image is generated and composited using an alpha image that models attenuation in the atmosphere. The use of the alpha image ensures that the intensity of the stars is correctly reduced due to scattering and absorption in the atmosphere. The alpha map records for every pixel the visibility of objects beyond the atmosphere. It is generated by the ray tracer as a secondary image. Each time a ray from the camera leaves the atmosphere, the transmitivity is stored in the alpha image. The star image is multiplied by the alpha image and added to the rendered image to produce the final image.

For star clusters, such as the Milky Way, where individual stars are not visible, we use a high resolution (14400x7200) photographic mosaic of the Night Sky [25]. The brightest stars were removed using pattern-matching and median filtering.

5.2 Color and Brightness of Stars

A stellar magnitude describes the apparent star brightness. Given the visual magnitude, the irradiance at the Earth is [21]:

$$E_s = 10^{0.4(-m_v - 19)}\ \frac{W}{m^2}. \tag{6}$$

For the Sun, $m_v \approx -26.7$; for the full Moon, $m_v \approx -12.2$; and for Sirius, the brightest star, $m_v \approx -1.6$. The naked eye can see stars with a stellar magnitude up to approximately 6. However, this is the visible magnitude, which takes into account the atmospheric scattering. Since we simulate atmospheric scattering, we must discount this absorption, which accounts for 0.4 magnitude:

$$E_s' = 10^{0.4(-m_v - 19 + 0.4)}\ \frac{W}{m^2}. \tag{7}$$

The color of the star is not directly available as a measured spectrum. Instead, astronomers have established a standard series of measurements in particular wave-bands. A widely used *UBV system* introduced by Johnson [18] isolates bands of the spectrum in the blue intensity B, yellow-green intensity V, and ultra-violet intensity U. The difference $B - V$ is called the *color index* of a star, which is a numerical measurement of the color. A negative value of $B-V$ indicates a more bluish color, while a positive value indicates a redder hue. UBV is not directly useful for rendering purposes. However, we can use the color index to estimate a star's temperature [33, 40]:

$$T_{eff} = \frac{7000K}{B - V + 0.56}. \tag{8}$$

To compute spectral irradiance from a star given T_{eff}, we first compute a non-spectral irradiance value from the stellar magnitude using Equation 7. We then use the computed value to scale a normalized spectrum based on Planck's radiation law for black body radiators [39]. The result is spectral irradiance.

In the color pages (Figure 9) we have rendered a close-up of stars. We use the physically-based glare filter by Spencer et al. [41] as a flare model for the stars. This model fits nicely with the observations by Navarro and Losada [28] regarding the shape of stars as seen by the human eye.

Figure 10 is a time-lapse rendering of stars. Here we have simulated a camera and omitted the loss of color by a human observer. The colors of the stars can be seen clearly in the trails. Notice, also the circular motion of the stars due to the rotation of the Earth.

5.3 Illumination from Stars

Even though many stars are not visible to the naked eye, there is a collective contribution from all stars when added together. We use a constant irradiance of $3 \cdot 10^{-8} \frac{W}{m^2}$ [38] to account for integrated starlight.

6 Other Elements

A variety of phenomena affect the appearance of the night sky in subtle ways. While one might assume the sky itself is colored only by scattered light in the atmosphere, that is in fact only one of four specific sources of diffuse visible color in the night sky. The other three are zodiacal light, airglow, and galactic/cosmic light. We include all of these in our model. These effects are especially important on moonless nights, when a small change in illumination can determine whether an object in the scene is visible or invisible.

6.1 Zodiacal Light

The Earth co-orbits with a cloud of dust around the Sun. Sunlight scatters from this dust and can be seen from the Earth as *zodiacal light* [5, 36]. This light first manifests itself in early evening as a diffuse wedge of light in the southwestern horizon and gradually broadens with time. During the course of the night the zodiacal light becomes wider and more upright, although its position relative to the stars shifts only slightly [2].

The structure of the interplanetary dust is not well-understood. To to simulate zodiacal light we use a table with measured values [38]. Whenever a ray exits the atmosphere, we convert the direction of the ray to ecliptic polar coordinates and perform a bilinear lookup in the table. This works well since zodiacal light changes slowly with direction and has very little seasonal variation. A result of our zodiacal light model is illustrated Figure 8.

6.2 Airglow

Airglow is faint light that is continuously emitted by the entire upper atmosphere with a main concentration at an elevation of approximately 110 km. The upper atmosphere of the Earth is continually being bombarded by high energy particles, mainly from the Sun. These particles ionize atoms and molecules or dissociate molecules and in turn cause them to emit light in particular spectral lines (at discrete wavelengths). As the emissions come primarily from Na and O atoms as well as molecular nitrogen and oxygen the emission lines are easily recognizable. The majority of the airglow emissions occur at 557.7nm (O-I), 630nm (O-I) and a 589.0nm - 589.6nm doublet (Na-I). Airglow is the principal source of light in the night sky on moonless nights.

Airglow is integrated into the simulation by adding an active layer to the atmosphere (altitude 80km) that contributes a spectral in-scattered radiance ($5.1 \cdot 10^{-8} \frac{W}{m^2}$, 3 peaks, at 557.7nm, 583.0nm and 630.0nm).

6.3 Diffuse Galactic Light and Cosmic Light

Diffuse galactic light and cosmic light are the last components of the night sky that we include in our model. These are very faint (see Figure 2) and modeled as a constant term ($1 \cdot 10^{-8} \frac{W}{m^2}$) that is added when a ray exits the atmosphere.

6.4 Atmosphere Modeling

Molecules and aerosols (dust, water drops and other similar-sized particles) are the two main constituents of the atmosphere that affect light. As light travels through the atmosphere it can be scattered by molecules (Rayleigh scattering) or by aerosols (Mie scattering). The probability that a scattering event occurs is proportional to the local density of molecules and aerosols and the optical path length of the light. The two types of scattering are very different: Rayleigh scattering is strongly dependent on the wavelength of the light and it scatters almost diffusely; aerosol scattering is mostly independent of the wavelength, but with a strong peak in the forward direction of the scattered light.

We model the atmosphere using a spherical model similar to that of Nishita et al. [29, 31] and use the same phase functions to approximate the scattering of light. To simulate light transport with multiple scattering, we use distribution ray tracing combined with ray marching. A ray traversing the atmosphere uses ray marching to integrate the optical depth, and it samples the in-scattered indirect radiance at random positions in addition to the direct illumination. Each ray also keeps track of the visibility of the background, and all rays emanating from the camera save this information in the alpha image (as discussed in Section 5.1). This method is fairly efficient because the atmosphere is optically thin. Also, the method is very flexible and allows us to integrate other components in the atmosphere such as clouds and airglow.

We model clouds procedurally using an approach similar to the one described in [9]. Clouds are similar to the atmosphere, but as they have a higher density, the number of scattering events will be larger. For clouds we use the Henyey-Greenstein phase-function [13] with strong forward scattering.

7 Implementation and Results

We implemented our night sky model in a Monte Carlo ray tracer with support for spectral sampling. We used an accurate spectral sampling with 40 evenly-spaced samples from 340nm to 740nm to allow for precise conversion to XYZV color space for tone mapping, as well as for accurately handling the wavelength dependent Rayleigh scattering of the sky. Simpler models could be used as well, at the expense of accuracy.

Because our scenes are at scotopic viewing levels (rod vision), special care must be taken with tone mapping. We found the histogram-adjustment method proposed by Ward et al. [22] to work best for the very high dynamic range night images. This method "discounts" the empty portions of the histogram of luminance, and simulates both cone (daylight) and rod (night) vision as well as loss of acuity. Another very important component of our tone-mapping model is the blue-shift (the subjective impression that night scenes exhibit a bluish tint). This phenomena is supported by psychophysical data [15] and a number of techniques can be used to simulate it [8, 17, 43]. We use the technique for XYZV images as described in [17].

Many features of our model have been demonstrated through the paper. Not all of the elements can be seen simultaneously in one image. In particular, the dimmest phenomena such as zodiacal light are visible only for moonless nights. Phenomena such as airglow and intergalactic light are present only as faint background illumination. Nonetheless, all these components are important to give a realistic impression of the night sky. The sky is never completely black.

Our experimental results are shown in the two color pages at the end of the paper. The captions explain the individual images. All the images were rendered on a dual PIII-800 PC, and the rendering time for most of the individual images ranged from 30 seconds to 2 minutes. It may seem surprising that multiple scattering in the atmosphere can be computed this quickly. The main reason for this is that multiple scattering often does not contribute much and as such can be computed with low accuracy — as also demonstrated in [29]. The only images that were more costly to render are the images with clouds; we use path tracing of the cloud media and this is quite expensive. As an example the image of Little Matterhorn [35] with clouds (Figure 13) took 2 hours to render.

A very important aspect of our images is the sense of night. This is quite difficult to achieve, and it requires carefully ensuring correct physical values and using a perceptually based tone-mapping algorithm. This is why we have stressed the use of accurate radiometric values in this paper. For a daylight simulation it is less noticeable if the sky intensity is wrong by a factor two, but in the night sky all of the components have to work together to form an impression of night.

8 Conclusions and Future Work

This paper has presented a physically-based model of the night sky. The model uses astronomical data and it includes all the significant sources of natural light in the night sky. We simulate the direct appearance of the Moon, stars, the Milky Way, the zodiacal light, and other elements. In addition we model the illumination from these sources of light including scattering in the atmosphere. Finally, we use accurate spectral sampling and tone-mapping in order to render convincing images of night scenes.

Our model suggests several interesting areas for future work. Additional optical effects that we would like to include involve the modeling of small discrepancies, such as the hiding effect that causes the Full Moon to be brighter than expected, the luminescence of the Moon due to ionization caused by solar particles, and the seasonal and diurnal variations of airglow. More work remains

to be done to accurately incorporate artificial light sources, city glow, and light pollution [26].

Tone mapping for night and twilight scenes presents many challenges. The complex interaction between rods and cones results in non-linear phenomena, in particular for brightness and color perception. Reproducing the alteration of motion perception at night is yet another topic for future work.

Acknowledgments

Thanks to Pat Hanrahan for several insightful comments, to Marc Levoy for last-minute creative suggestions, to Axel Mellinger for his full-resolution Milky Way mosaic, to Stephen Duck for modeling the night city skyline and to Frank Stark and Maryann Simmons for a conscientious read back. Additional thanks to Max Chen, Claus Wann Jensen, Steve Marschner, Ministry, Les Norford, and Byong Mok-Oh. The work of the first author was supported in part by NSF/ITR (IIS-0085864) and DARPA (DABT63-95-C-0085). In addition this work was supported by the NSF Science and Technology Center for Computer Graphics and Scientific Visualization (ASC-89-20219), an NSF CISE Research Infrastructure award (EIA09802220), an NSF grant (97-31859), and a gift from Pixar Animation Studios.

Appendix

In this Appendix we present formulas for coordinate conversion and low-precision formulas for the positions of the Sun and Moon. The formulas are adapted from [10, 23, 24, 44]. All the angles are in radians, unless otherwise noted. R_x, R_y and R_z are the standard counter-clockwise rotation matrices about the principal axes.

Time Conversion

Astronomers often use *Julian dates*. For the date $M/D/Y$ ($Y > 1582$) at time $h{:}m{:}s$ ($0 \le h < 24$), the Julian date is given by

$$\begin{aligned} JD &= 1720996.5 - \lfloor Y'/100 \rfloor + \lfloor Y'/400 \rfloor + \lfloor 365.25Y' \rfloor \\ &\quad + \lfloor 30.6001(M'+1) \rfloor + D + (h + (m + s/60)/60)/24 \end{aligned}$$

where Y' and M' are the adjusted year and month: if M is 1 or 2, then $Y' = Y - 1$ and $M' = M + 12$ otherwise $Y' = Y$ and $M' = M$. $\lfloor\ \rfloor$ denotes the floor integer truncation function.

Local time is GMT with a zone correction. *Terrestrial Time* (TT) is essentially the time kept by atomic clocks. As it is not corrected for the slowing of the Earth's rotation, it gains on GMT by about a second per year. The current difference ΔT is about 65 sec. It should be added to s in Equation (9) above for precise computation.

The variable T in this Appendix is the time in Julian centuries since January 1, 2000: $T = (JD - 2451545.0)/36525$.

Coordinate Conversion

Coordinate conversion is most easily done in rectangular coordinates using rotation matrices. The generic rectangular conversion is:

$$\begin{aligned} x &= r\cos(\text{longitude})\cos(\text{latitude}) \\ y &= r\sin(\text{longitude})\cos(\text{latitude}) \\ z &= r\sin(\text{latitude}). \end{aligned} \tag{10}$$

A point in ecliptic coordinates may be converted to equatorial coordinates using the matrix $R_x(\epsilon)$, where ϵ is the *obliquity of the ecliptic*. The mean value in radians is $\epsilon = 0.409093 - 0.000227T$, with T as above.

Converting to local horizon coordinates is harder. The rotation of the Earth is abstracted by the *local sidereal time* of an observer, which when measured in angular hours (1 hour = 15 degrees) gains about 4 arc-minutes a day on local solar time. If lon is the observer's longitude in radians (East is positive), the local mean sidereal time, in radians, is given by $\text{LMST} = 4.894961 + 230121.675315T + \text{lon}$. Here T is as above, but in GMT *without* the correction ΔT. All other formulas in this Appendix assume the ΔT correction has been included in the computation of T.

The matrix for converting mean equatorial coordinates to horizon coordinates is $R_y(lat - \pi/2)R_z(-\text{LMST})P$, where lat is the observer's latitude in radians, positive to the North. P is a rotation matrix that corrects for precession and nutation. The effect of precession is about one degree per century, so P can be omitted near 2000. For precession only, P is approximately $P = R_z(0.01118T)R_y(-0.00972T)R_z(0.01118T)$. Nutation never amounts to more than about 20 arc-seconds.

Position Computations

We conclude by giving low precision formulas for the position of the Sun and the Moon. The formulas are for the ecliptic longitude and latitude (λ, β) corrected for precession. The Sun position formula is accurate to about one arc-minute within five centuries of 2000; and the Moon position formula is accurate to better than eight arc-minutes within five centuries of 2000.

Sun

For the coordinates of the sun, compute $M = 6.24 + 628.302T$,

$$\begin{aligned} \lambda &= 4.895048 + 628.331951T + (0.033417 - 0.000084T)\sin M \\ &\quad + 0.000351\sin 2M, \\ r &= 1.000140 - (0.016708 - 0.000042T)\cos M - 0.000141\cos 2M, \end{aligned}$$

and $\beta = 0$. The geocentric distance r is in astronomical units (1au = 1.496×10^{11}m = 23455 Earth radii.) For the position in local horizon coordinates, convert to rectangular coordinates, then rotate using the matrix $R_y(lat - \pi/2)R_z(-\text{LMST})R_x(\epsilon)$.

Moon

The ecliptic geocentric coordinates of the Moon are computed from

$$\begin{aligned} l' &= 3.8104 + 8399.7091T & m' &= 2.3554 + 8328.6911T \\ m &= 6.2300 + 628.3019T & d &= 5.1985 + 7771.3772T \\ f &= 1.6280 + 8433.4663T \end{aligned}$$

$$\begin{aligned} \lambda = {} & l' \\ & +0.1098\sin(m') \\ & +0.0222\sin(2d - m') \\ & +0.0115\sin(2d) \\ & +0.0037\sin(2m') \\ & -0.0032\sin(m) \\ & -0.0020\sin(2f) \\ & +0.0010\sin(2d - 2m') \\ & +0.0010\sin(2d - m - m') \\ & +0.0009\sin(2d + m') \\ & +0.0008\sin(2d - m) \\ & +0.0007\sin(m' - m) \\ & -0.0006\sin(d) \\ & -0.0005\sin(m + m') \end{aligned}$$

$$\begin{aligned} \beta = {} & +0.0895\sin(f) \\ & +0.0049\sin(m' + f) \\ & +0.0048\sin(m' - f) \\ & +0.0030\sin(2d - f) \\ & +0.0010\sin(2d + f - m') \\ & +0.0008\sin(2d - f - m') \\ & +0.0006\sin(2d + f) \end{aligned}$$

$$\begin{aligned} \pi' = {} & +0.016593 \\ & +0.000904\cos(m') \\ & +0.000166\cos(2d - m') \\ & +0.000137\cos(2d) \\ & +0.000049\cos(2m') \\ & +0.000015\cos(2d + m') \\ & +0.000009\cos(2d - m) \end{aligned}$$

The distance is $d_{\text{Moon}} = 1/\pi'$ in units of Earth radii. To correct for the observer's position on the Earth, convert to rectangular coordinates and to local horizon coordinates as for the sun. Then subtract the vector $(0, 0, 1)$, the approximate position of the observer in horizon coordinates.

Rotation and Phase of the Moon

The Moon's geometry is modeled in a fixed lunar coordinate system. To orient the Moon in ecliptic coordinates, rotate by the matrix $R_z(f+\pi)R_x(0.026920)R_z(l'-f)$, with f as above. Then rotate by the equatorial to horizon conversion matrix for the orientation in horizon coordinates. Translating by the Moon's position in rectangular horizon coordinates (scaled by 6378137m) completes the position and orientation of the Moon in local horizon coordinates.

Using rectangular coordinates makes it easy to compute the position of the shadow terminator. If $\vec{m}$ is the topocentric position of the Moon, and $\vec{s}$ is that of the sun (in Earth radii: multiply d_{Moon} above by 23455; there is no need to correct for parallax for the sun's position) then the vector $(\vec{s}-\vec{m})\times(\vec{s}\times\vec{m})$ points from the center of the Moon to the leading (light to dark) terminator.

Temperature to Luv Conversion

Temp. (K)	u	v	Temp. (K)	u	v
100 000	0.18065	0.26589	4000	0.22507	0.33436
50000	0.18132	0.26845	3636	0.23243	0.33901
33333	0.18208	0.27118	3333	0.24005	0.34305
25000	0.18293	0.27407	3077	0.24787	0.34653
20000	0.18388	0.27708	2857	0.25585	0.34948
16667	0.18494	0.28020	2667	0.26394	0.35198
14286	0.18611	0.28340	2500	0.27210	0.35405
12500	0.18739	0.28666	2353	0.28032	0.35575
11111	0.18879	0.28995	2222	0.28854	0.35713
10000	0.19031	0.29325	2105	0.29676	0;35822
8000	0.19461	0.30139	2000	0.30496	0.35906
6667	0.19960	0.30918	1905	0.31310	0.35968
5714	0.20523	0.31645	1818	0.32119	0.36011
5000	0.21140	0.32309	1739	0.32920	0.36038
4444	0.21804	0.32906	1667	0.33713	0.36051

References

[1] BARANOSKI, G., ROKNE, J., SHIRLEY, P., TRONDSEN, T., AND BASTOS, R. Simulating the aurora borealis. In *Proc. of Pacific Graphics* (2000).

[2] BLACKWELL, D. E. The zodiacal light. *Scientific American 54* (July 1960).

[3] BLINN, J. The jupiter and saturn fly-by animations, 1980.

[4] BLINN, J. F. Light reflection functions for simulation of clouds and dusty surfaces. *Proc. of SIGGRAPH* (1982).

[5] DERMOTT, S. F., AND LIOU, J. C. Detection of asteroidal dust particles from known families in near-earth orbits. In *AIP Conference Proceedings* (July 1994), vol. 301(1), pp. 13–21.

[6] DOBASHI, Y., NISHITA, T., KANEDA, K., AND YAMASHITA, H. A fast display method of sky colour using basis functions. *J. of Visualization and Computer Animation 8*, 3 (Apr. – June 1997), 115–127.

[7] DUFFETT-SMITH, P. *Astronomy with your personal computer*, 2nd ed. Cambridge University Press, 1990.

[8] DURAND, F., AND DORSEY, J. Interactive tone mapping. *Eurographics Workshop on Rendering* (2000).

[9] EBERT, D., MUSGRAVE, K., PEACHEY, D., PERLIN, K., AND WORLEY, S. *Texturing and Modeling: A procedural Approach*. Academic Press, 1994.

[10] GREEN, R., Ed. *Spherical Astronomy*. Cambridge Univ. Pr., 1985.

[11] HAPKE, B. Optical properties of the lunar surface. In *Physics and astronomy of the Moon*, Kopal, Ed. Academic Press, 1971.

[12] HAPKE, B. W. A theoretical photometric function of the lunar surface. *Journal of Geophysical Research 68*, 15 (1963), 4571–4586.

[13] HENYEY, L. G., AND GREENSTEIN, J. L. Diffuse radiation in the galaxy. *Astrophysics Journal 93* (1941), 70–83.

[14] HOFFLEIT, D., AND WARREN, W. *The Bright Star Catalogue*, 5th ed. Yale University Observatory, 1991.

[15] HUNT. Light and dark adaptation and the perception of color. *Journal of the Optical Society of Am. A 42*, 3 (1952), 190.

[16] J. VAN DIGGELEN. Photometric properties of lunar carter floors. *Rech. Obs. Utrecht 14* (1959), 1–114.

[17] JENSEN, H. W., PREMOZE, S., SHIRLEY, P., THOMPSON, W., FERWERDA, J., AND STARK, M. Night rendering. Tech. Rep. UUCS-00-016, Computer Science Dept., University of Utah, Aug. 2000.

[18] JOHNSON, H. L., AND MORGAN, W. W. Fundamental stellar photometry for standards of spectral type on the revised system of the yerkes spectral atlas. *Astrophysics Journal 117*, 313 (1953).

[19] KLASSEN, R. Modeling the effect of the atmosphere on light. *ACM Trans. on Graphics 6*, 3 (1987), 215–237.

[20] KOPAL, Z. *The Moon*. D. Reidel Publishing Company, Dordrecht, Holland, 1969.

[21] LANG, K. Astrophysical formulae. *Astronomy and astrophysics library* (1999).

[22] LARSON, G. W., RUSHMEIER, H., AND PIATKO, C. A visibility matching tone reproduction operator for high dynamic range scenes. *IEEE Trans. on Visualization and Computer Graphics 3*, 4 (Oc. - Dec. 1997), 291–306.

[23] MEEUS, J. *Astronomical Formulae for Calculators*, 4th ed. Willman-Bell, Inc., 1988.

[24] MEEUS, J. *Astronomical Algorithms*, 2nd ed. Willmann-Bell, Inc., Richmond, VA, 1999.

[25] MELLINGER, A. A 360°x180° all-sky panorama. http://canopus.physik.uni-potsdam.de/˜axm/images.html, 2000.

[26] MINNAERT, M. *Light and Color in the Outdoors*. Springer-Verlag, 1974.

[27] NAVAL RESEARCH LABORATORY. Clementine deep space program science experiment. http://www.nrl.navy.mil/clementine/.

[28] NAVARRO, R., AND LOSADA, M. A. Shape of stars and optical quality of the human eye. *Journal of the Optical Society of America (A) 14*, 2 (1997), 353–359.

[29] NISHITA, T., DOBASHI, Y., KANEDA, K., AND YAMASHITA, H. Display method of the sky color taking into account multiple scattering. In *Proc. of Pacific Graphics* (1996).

[30] NISHITA, T., AND NAKAMAE, E. Continuous tone representation of three-dimensional objects illuminated by sky light. In *Computer Graphics (SIGGRAPH '86 Proceedings)* (1986), vol. 20(4).

[31] NISHITA, T., SIRAI, T., TADAMURA, K., AND NAKAMAE, E. Display of the earth taking into account atmospheric scattering. In *Computer Graphics (SIGGRAPH '93 Proceedings)* (1993), vol. 27.

[32] OBERSCHELP, W., AND HORNUG, A. Visualization of eclipses and planetary conjunction events. the interplay between model coherence, scaling and animation. In *Proc. of Computer Graphics International* (2000).

[33] OLSON, T. The colors of the stars. In *IST/SID 6th Color Imaging Conf.* (1998).

[34] PREETHAM, A. J., SHIRLEY, P., AND SMITS, B. A practical analytic model for daylight. In *Proc. of SIGGRAPH* (1999).

[35] PREMOZE, S., THOMPSON, W., AND SHIRLEY, P. Geospecific rendering of alpine terrain. In *Eurographics Workshop on Rendering* (1999).

[36] REACH, W. T., FRANZ, B. A., KELSALL, T., AND WEILAND, J. L. Dirbe observations of the zodiacal light. In *AIP Conference Proceedings* (January 1996), vol. 348, pp. 37–46.

[37] RICHTER, N. B. The photometric properties of interplanetary matter. *Quarterly Journal of the Royal Astronomical Society 3* (1962), 179–186.

[38] ROACH, F., AND GORDON, J. *The Light of the Night Sky*. Geophysics and Astrophysics Monographs, V. 4. D Reidel Pub Co, 1973.

[39] SIEGEL, R., AND HOWELL, J. R. *Thermal Radiation Heat Transfer*, 3rd ed. Hemisphere Publishing Corporation, 1992.

[40] SMITH, R. C. *Observational Astrophysics*. Cambridge University Press, 1995.

[41] SPENCER, S., SHIRLEY, P., ZIMMERMAN, K., AND GREENBERG, D. Physically-based glare effects for digital images. In *Computer Graphics (Proc. Siggraph)* (1995).

[42] TADAMURA, K., NAKAMAE, E., KANEDA, K., BABA, M., YAMASHITA, H., AND NISHITA, T. Modeling of skylight and rendering of outdoor scenes. In *Eurographics '93* (1993), Blackwell Publishers.

[43] UPSTILL, S. *The Realistic Presentation of Synthetic Images: Image Processing in Computer Graphics*. PhD thesis, Berkeley, 1985.

[44] U.S. NAVAL OBSERVATORY, R. G. O. *The Astronomical Almanac for the Year 2001*. U.S. Government Printing Office, 2001.

[45] VAN DE HULST, H. *Light Scattering by Small Particles*. Wiley & Sons, 1957.

[46] VAN DE HULST, H. *Multiple Light Scattering*. Academic Press, 1980.

[47] YAEGER, L., UPSON, C., AND MYERS, R. Combining physical and visual simulation – creation of the planet jupiter for the film "2010". *Proc. of SIGGRAPH)* (1986).

Figure 7: The Moon rendered at different times of the month and day and under different weather conditions. Clockwise from top left. The sliver moon is a simulation of the moon on Dec. 5; Earthshine makes all of the moon visible. The Quarter Moon (Dec. 12) is a day simulation and the moon is seen behind the blue sky. The Gibbous Moon (Dec. 17) is a rendering of the moon low in the sky; it is colored red/orange due to attenuation in the atmosphere of the blue part of the light. The full moon (Dec. 22) is a simulation of the moon seen through a thin layer of clouds with strong forward scattering; the scattering in the cloud causes the bright region around the moon.

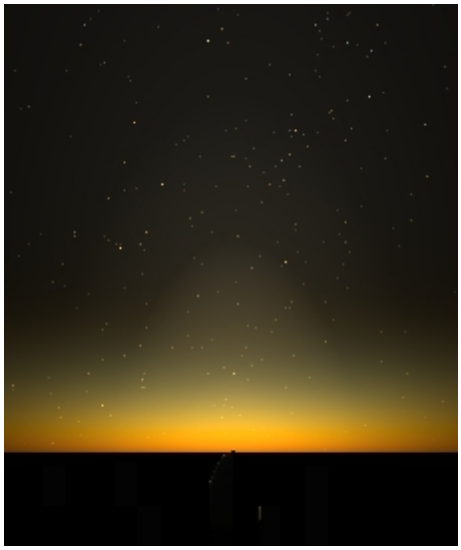

Figure 8: Zodiacal light seen as a wedge of light rising from the horizon in an early autumn morning. Zodiacal light is easiest to see on spring evenings and autumn mornings from the Northern hemisphere.

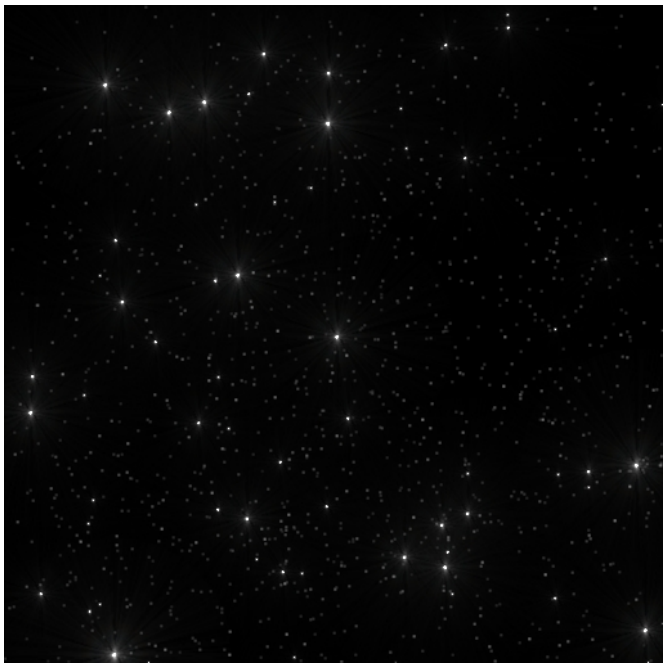

Figure 9: Close-up of rendered stars. Note the glare simulation around the brighter stars. The Big Dipper (in the constellation of Ursa Major) is clearly recognizable at the top of the image.

Figure 10: Time-lapse rendering of stars. A simulation of a 30-minute camera exposure of the sky. Note how the stars move in circular curves due to the rotation of the earth. Also, note the color of the stars (we did not apply tone-mapping for a human observer, and the true colors of the stars are seen in the trails).

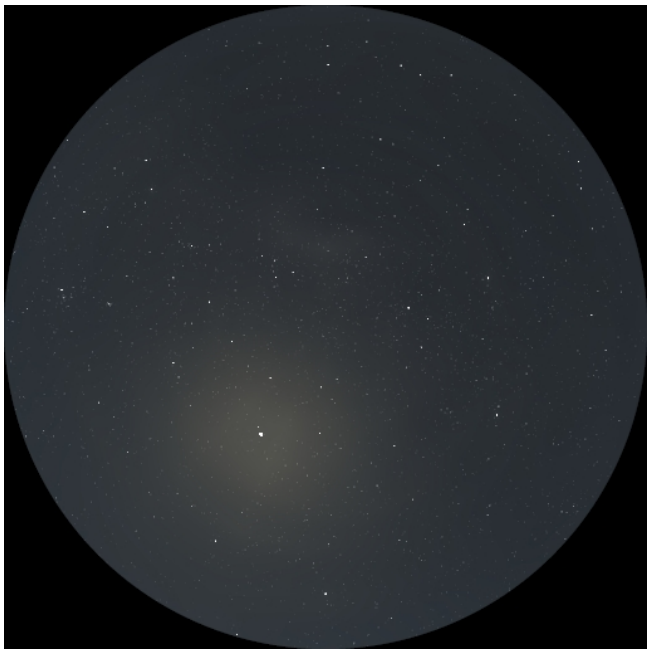

Figure 11: Fisheye lens projection of a hazy night sky illuminated by the full moon. Note the scattering in the atmosphere around the moon. Note also the Big Dipper near the top of the image.

Figure 12: Moon rising above a mountain ridge. The only visible feature in this dark night scene is the scattering of light in the thin cloud layer.

Figure 13: A simulation of Little Matterhorn illuminated by the full moon on a clear night. Notice how the tone-mapping combined with the blue shift give a sense of night.

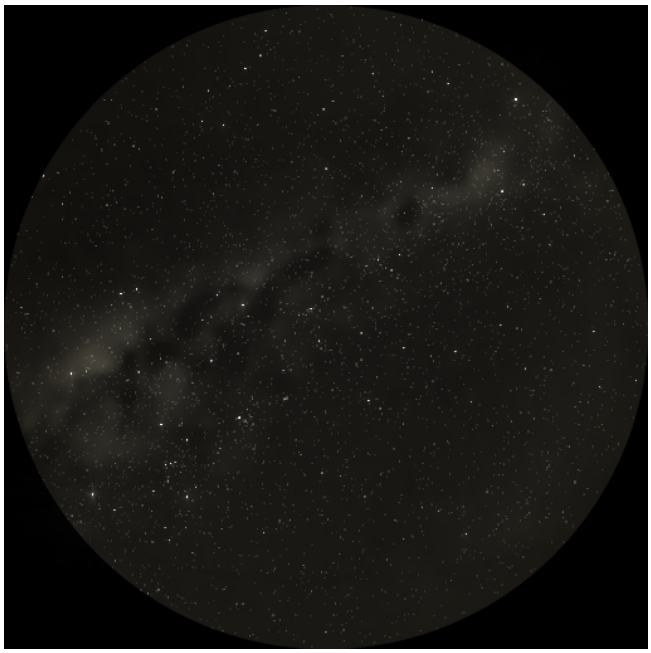

Figure 14: Fisheye lens projection of a clear moonless night. The Milky Way band is visible across the sky as are the dimmer stars. The Orion constellation can be seen at the lower left of the image.

Figure 15: The low moon setting over a city skyline in the early morning. The red sky is illuminated via multiple scattering from the low rising sun.

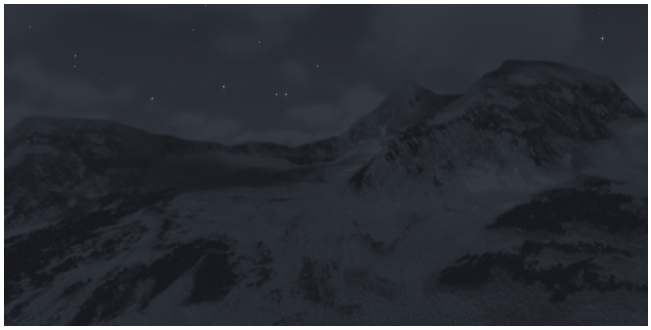

Figure 16: A simulation of Little Matterhorn illuminated by a full moon on a cloudy night sky. Note the reduced visibility of the stars as well as the shadows of the clouds on the mountain.